Buckling Testing of a Subscale Composite Cylinder

Rudd, Michelle Tillotson; Schultz, Marc R.; Waters, W. Allen; Gardner, Nathaniel W.; Bisagni, C.

DOI
10.2514/6.2021-0205

Publication date
2021

Document Version
Final published version

Published in
AIAA Scitech 2021 Forum

AIAA SciTech Forum
11–15 & 19–21 January 2021, VIRTUAL EVENT
AIAA Scitech 2021 Forum

10.2514/6.2021-0205

Buckling Testing of a Subscale Composite Cylinder

Michelle Tillotson Rudd[1]
NASA Marshall Space Flight Center, Huntsville, AL, 35812

Marc R. Schultz[2]
NASA Langley Research Center, Hampton, VA 23681

W. Allen Waters[3]
Analytical Mechanics Associates, Hampton, VA 23666

Nathaniel W. Gardner[4]
Analytical Services and Materials, Inc., Hampton, VA, 23666

Chiara Bisagni[5]
Delft University of Technology, Delft, 2629HS, Netherlands

A subscale solid laminate composite cylinder with a 31.5-in. diameter, a 48.2-in. length, and a $[23/0/-23]_{4S}$ layup was designated NDL-1 and was designed to fail in buckling after a series of subcritical tests. NDL-1 was experimentally loaded in axial compression until buckling at 466.3 kips. Visual inspection of the test article after the test revealed that a shallow area of delamination occurred near the buckling initiation site. After a successful first buckling test, there was an opportunity to test NDL-1 in axial compression to failure a second time despite that the test article was not designed or analyzed for multiple buckling tests. During the second test to failure, NDL-1 reached a peak load of 390.4 kips, 16.3% lower than the first test. Buckling did not initiate in the same location during the second test to failure as the first test to failure. The second buckling event caused a large V-shaped crack that penetrated through the thickness of the barrel. Though buckling initiated at different locations, a similar radial deformation pattern was present just prior to buckling during the both tests. In the end, NDL-1 maintained a significant amount of its structural integrity and a similar prebuckling radial displacement pattern, even after the first buckling test.

Nomenclature

DCDT	=	Direct current differential transducers
DIC	=	Digital image correlation
IML	=	Inner mold line
NDL-1	=	NASA Delft Laminate-1, considered cylindrical composite test article
OML	=	Outer mold line
SBKF	=	Shell Buckling Knockdown Factor Project
TTF-1	=	First test to failure
TTF-2	=	Second test to failure

[1] Aerospace Engineer, Structural Design, Development, and Analysis Branch, EV32.
[2] Research Aerospace Engineer, Structural Mechanics & Concepts Branch, MS 190, AIAA Associate Fellow.
[3] Lead, Structural Mechanics and Analysis, supporting the Structural Mechanics & Concepts Branch, MS 190.
[4] Senior Scientist, supporting the Structural Mechanics & Concepts Branch, MS 190.
[5] Full Professor, Faculty of Aerospace Engineering, Kluyverweg 1, AIAA Associate Fellow.

I. Introduction

The Shell Buckling Knockdown Factor Project (SBKF) was established in 2007 by the NASA Engineering and Safety Center with the intent of developing a greater understanding of factors, such as radial and thickness imperfections, that influence the buckling response of thin-walled metallic and composite shells through analytical, numerical, and experimental investigation. To that end, SBKF collaborated with the Delft University of Technology to design and test a 31.5-in. diameter laminate composite cylinder to fail in buckling, referred to herein as NASA Delft Laminate-1 or NDL-1. The design of the test article was based on an analytical scaling methodology, that was developed for the design of lab-scale test articles to mimic the buckling behavior of large-scale buckling-critical cylindrical shells [1]. The primary objective of the NDL-1 testing was to load the test article in axial compression under various load levels including one final failure load sequence to understand the prebuckling, buckling, and postbuckling behavior.

The design and manufacturing of NDL-1 is presented in Section II. The test set up and results for the first test to failure, the second test to failure, and a comparison of the performance of the test article from the first and second test are discussed in Section III. Finally, a summary of the findings is given in Section IV.

II. Test Article Design and Manufacturing

Test article NDL-1 was a laminated composite cylinder fabricated from the Hexcel IM7/8552-1 (190 gsm) graphite-epoxy material system [2]. IM7/8552-1 is a toughened 350 °F cure material system and is a unidirectional tape with an average tape thickness of 0.0071 in. The in-plane lamina tensile elastic moduli and failure stresses for IM7/8552-1 material system are listed in Table 1 [3]. Assuming linear elastic behavior, the elastic moduli and failure stresses were used to calculate failure strains, Table 2. Without laminate material properties, the lamina properties provide a suitable reference point for material failure.

Table 1. IM7-8552 in plane lamina elastic moduli and failure stresses [3].

IM7-8552 Material Properties			
Longitudinal Tensile Modulus	E_1^t	20,435.82	ksi
Transverse Tensile Modulus	E_2^t	1,409.77	ksi
Longitudinal Compression Failure Stress	F_1^{cu}	251.06	ksi
Transverse Tensile Failure Stress	F_2^{tu}	9.29	ksi

Table 2. Calculated IM7-8552 lamina failure strains.

IM7-8552 Calculated Failure Strains			
Longitudinal Compression	ε_1^c	12280	με
Transverse Tension	ε_2^t	6584	με

This test article was fabricated using an advanced fiber placement robot at the NASA Marshall Space Flight Center Composites Technology Lab and designed to fail in buckling. The unidirectional tape plies were fiber placed on the outer surface of an aluminum cylindrical mandrel in the desired fiber orientation, with the 0 degree direction being parallel to the longitudinal axis and the 90 degree direction being oriented circumferentially. The inner mold line diameter was nominally 31.5 in, and the test article had a final trimmed length of 48.2 in. The acreage laminate was $[23/0/-23]_{4S}$ (24 plies, nominally 0.1704-in. total laminate thickness). Additional pad ups were included at the ends of the test article to assist with load introduction. Design details are included in Figure 1 and Table 3.

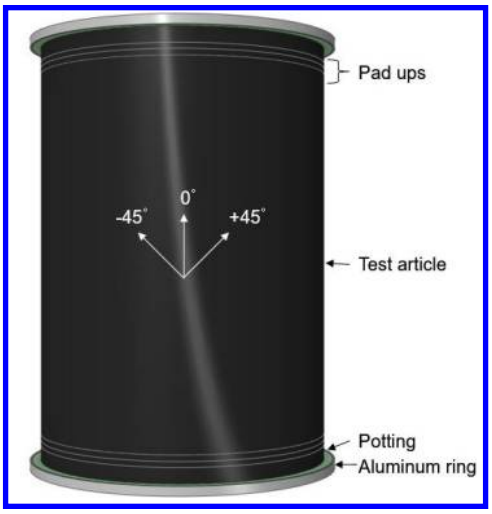

Figure 1. NDL-1 geometry and design details.

Table 3. NDL-1 acreage and pad up layup details.

Region	Layup	Axial station from midheight (0 in.) of pad up termination
Acreage	$[(23/0/-23)]_{S4}$	-
Pad up 1	$[(23/0/-23)_{S3}/(23/0/-23/\overline{90})_S]$	+/- 20.00
Pad up 2	$[(23/0/-23)_{S3}/-\overline{45}/(23/0/-23/\overline{90})_S]$	+/- 20.65
Pad up 3	$[(23/0/-23)_{S2}/(23/0/-23/\overline{45})_S/-45/(23/0/-23/\overline{90})_S]$	+/- 21.25

After manufacturing, the ends of the composite cylinder were encased in aluminum rings with an epoxy grout material to prevent brooming at the ends and attempt to simulate clamped boundary conditions. The grout was 1.0-in. thick on each end and extended approximately 0.90 in. away from the inner mold line (IML) and outer mold line (OML) surfaces of the composite cylinder. The IML and OML surfaces of the potting were encased in aluminum rings 0.25-in. thick to contain the grout material. The ends of the test article were machined flat and parallel with the shell exposed on either end to ensure uniform compressive load introduction.

After fabrication, NDL-1 was structured light scanned to capture the as-built geometry of the the test article. The IML and OML of the barrel were scanned and combined in a single coordinate system to allow determination of the midsurface radial location, as well as thickness imperfections. The midsurface radial locations are shown in Figure 2 in an unrolled view of NDL-1. The blue colors correspond to a relatively inward position, while the red colors correspond to a relatively outward position. The red-orange bands at the top and bottom of the figure are the thicker pad-ups regions. There is also a distinct feature approximately 2-in. wide that extends around the entire circumference of the test article centered about 5 in. above the midheight (0 in.). The aluminum mandrel which NDL-1 was built on was also structured light scanned after it was fabricated, and this feature was also present on the mandrel. It was determinined this feature was an artifact of the manufacturing process. The thickness variations of NDL-1 are presented in Figure 3 where the warmer colors correspond to thicker regions and the cooler colors denote realtively thinner regions. The diagonal pattern in Figure 3 matched the 23-degree ply angle and corresponds to ply gaps and overlaps.

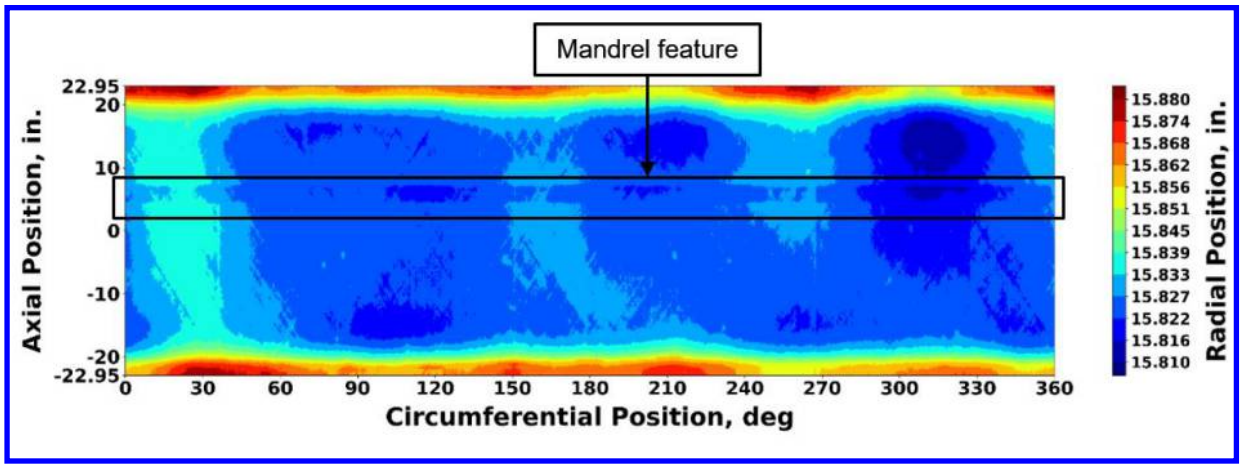

Figure 2. NDL-1 midsurface radial position.

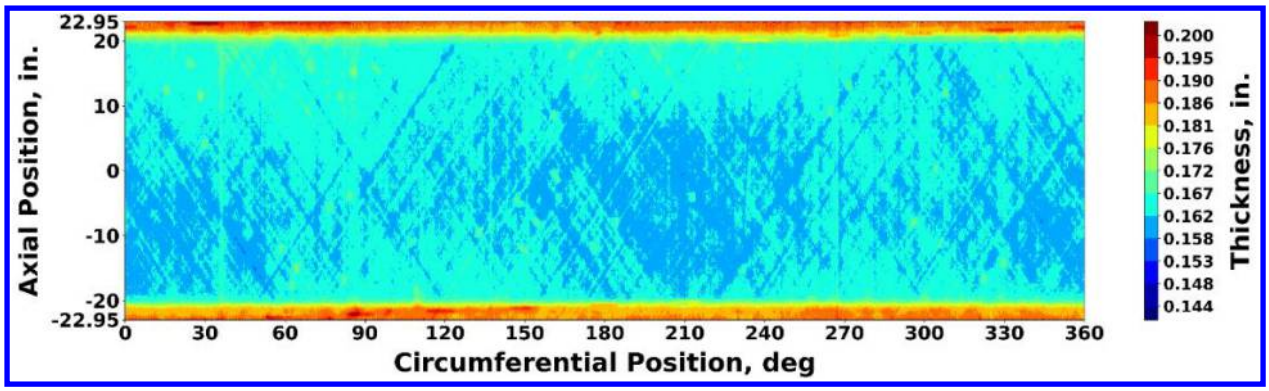

Figure 3. NDL-1 thickness variations.

III. Testing

A. First Test to Failure

The objective of the first test sequence was to load NDL-1 in uniform axial compression at various load levels to interrogate the prebuckling, buckling, and postbuckling response. The test was conducted in the Dr. James H. Starnes, Jr. Structures and Materials Research Laboratory at the NASA Langley Research Center, Hampton, VA. A number of measurement systems were used to monitor the test article such as, direct current displacement transducers (DCDTs), strain gages, low-speed Digital Image Correlation (DIC), high-speed video/DIC, and standard video. The experimental set up is shown in Figure 4.

NDL-1 was instrumented with traditional strain gages and displacement sensors to monitor the test article's behavior, as well as low-speed and high-speed DIC systems. Sixteen (16) axial strain gages were equally space around the circumference every 90 degrees at axial stations of -22.125 in. and 22.125 in. on the OML and IML. Eight (8) biaxial gauges were also spaced every 90 degrees at midheight on the OML and IML. Six (6) DCDTs were used to measure the relative displacement of the load frame and the test article. In addition to the strain gages and displacement sensors, DIC was used to derive full-field strain and displacement measurements during the test. To achieve this, four (4) low-speed and four (4) high-speed 3D DIC systems (note: each system consists of two cameras) were centered at 45, 135, 225, and 315 degrees. It is important to note that there were blind spots around the 90- and 270- degree circumferential location for the 3D DIC systems due to the load frame posts.

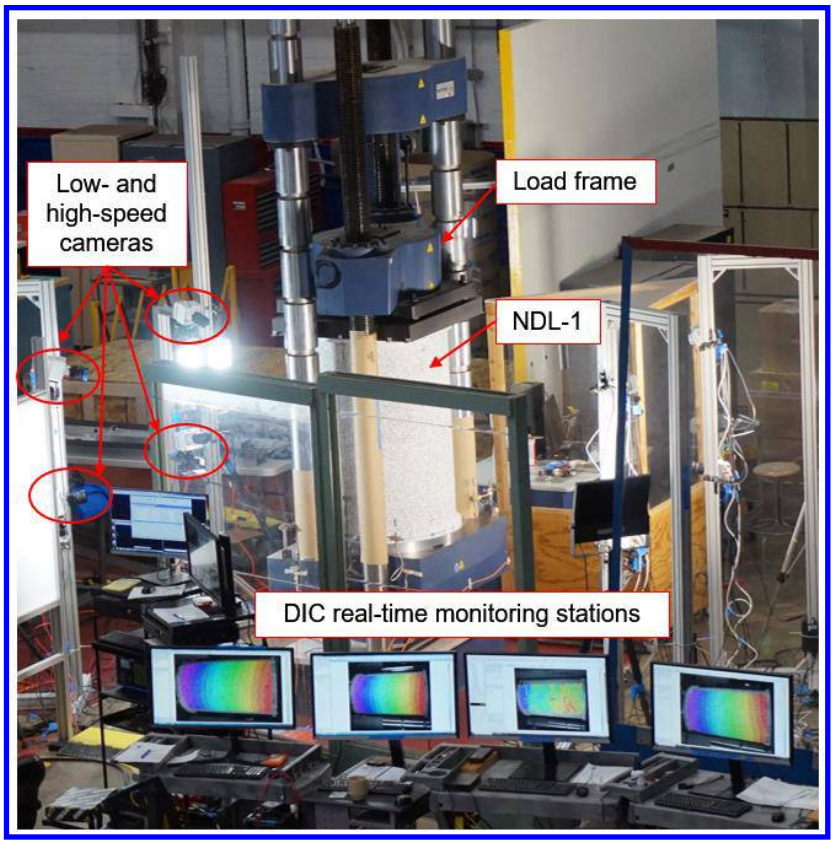

Figure 4. NDL-1 experimental setup.

Testing began with a set of subcritical load cases which applied axial compression to the barrel in increasingly high levels, but below the predicted failure load. The purpose of the subcritical load sequences was to ensure the barrel was behaving as expected and load was being applied to the test article adequately. Prior to the first test to failure, NDL-1 was loaded in axial compression to 100 kips once, then 200 kips twice, and finally 150 kips for a total of four subcritical load sequences.

The fifth and final load sequence, TTF-1, loaded the test article to a maximum axial load of 466.3 kips and a corresponding end shortening of 0.085 in. causing a buckling failure. Figure 5 shows the OML radial displacement, axial strain, and hoop strains in the test article just prior to buckling. Buckling initiated at a dimple approximately 5 in. above the midlength of the test article at the circumferential position of 200 degrees as seen in the radial displacement plot in Figure 5a. Figure 5a represents an unrolled view of the test article where the red colors indicate relative outward displacements and blue color indicate relative inward displacements. The location of the dimple is centered about the feature on NDL-1 caused by the mandrel imperfection as seen in Figure 2. Also, the maximum axial strain and hoop strain measured just prior to buckling as seen in Figure 5b and Figure 5c, -3004 με and -3403 με respectively, were less than the calculated failure strains in Table 2, -12280 με and 6584 με. Based on maximum strain criterion, it was concluded that the test article failed in buckling rather than a strength failure. It should be noted that a detailed description of the pretest predictions, test setup, and posttest analysis correlation for TTF-1 has been documented [4].

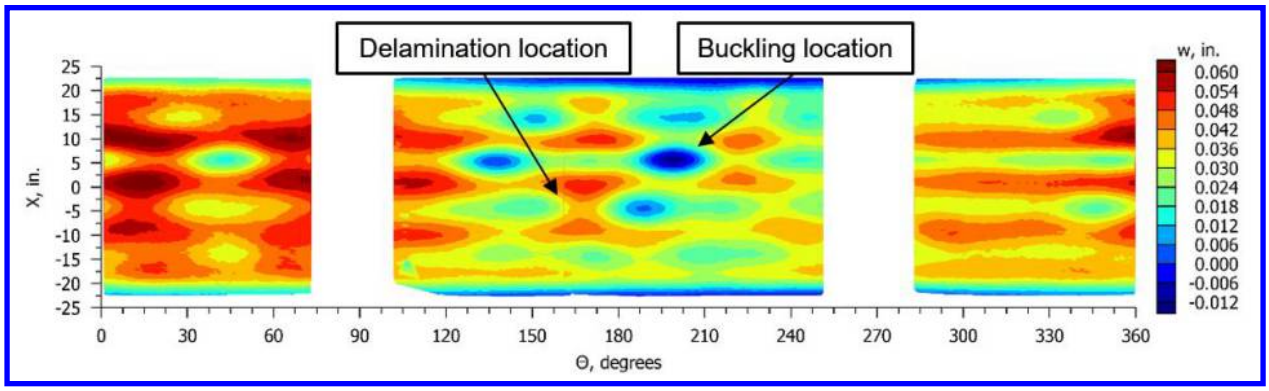

a.) Radial displacements.

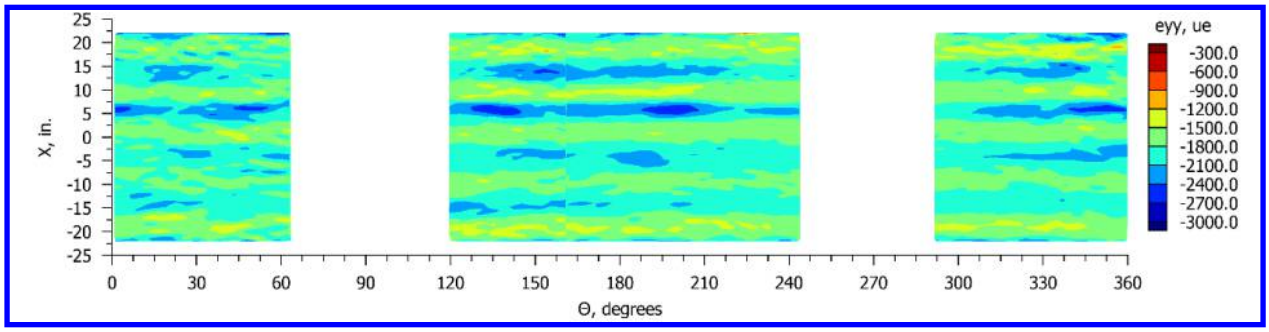

b.) Axial strain.

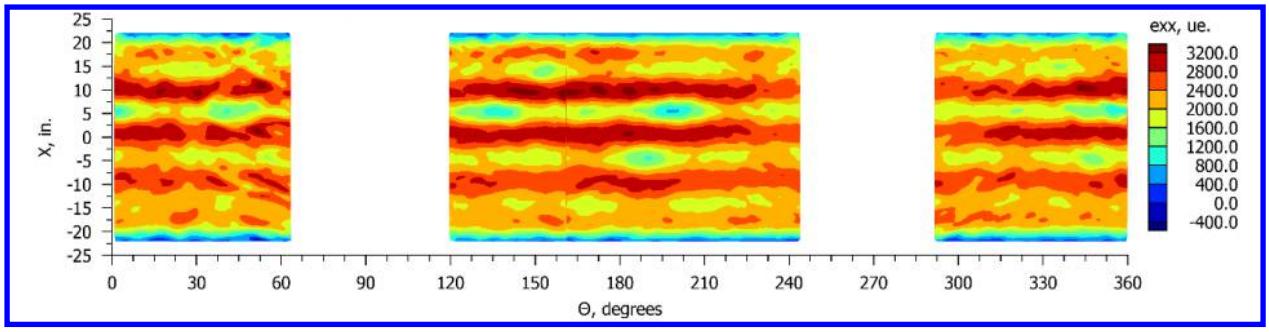

c.) Hoop strain.

Figure 5. NDL-1 at TTF-1 incipient failure.

A shallow delamination approximately 6-in. long and 2-in. wide was found by visually inspecting NDL-1 after TTF-1 at a circumferential location of 170 degrees, midheight, as indicated by the red outline on NDL-1 in Figure 6. The delamination occurred at an inflection point between an outward dimple and an adjacent relative inward dimple as seen in Figure 5a. The angle of the delamination is +23 degrees, which is the angle of the outer most ply. The depth of the delamination was not conclusive, but visual and ultrasonic inspection determined it was close to the OML.

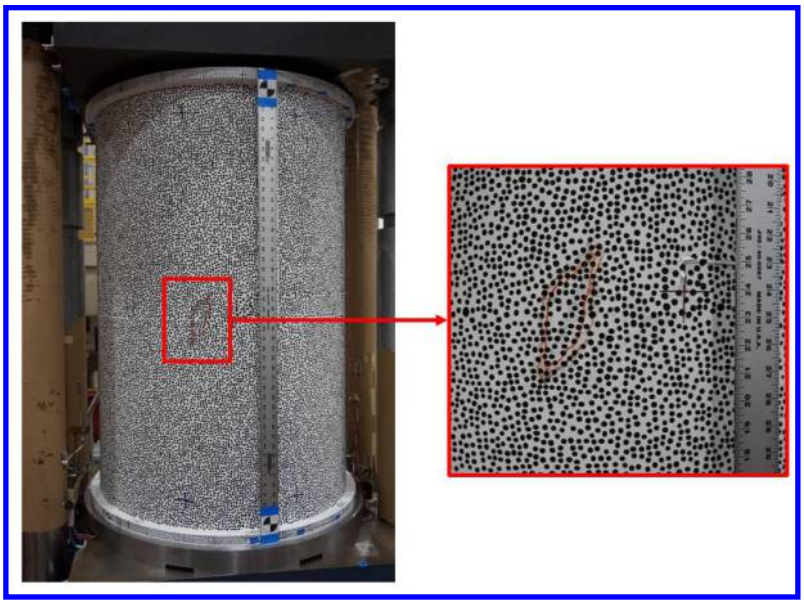

Figure 6. Delamination during the TTF-1 buckling event circled in red.

B. Second Test to Failure

While postprocessing the data from TTF-1, it was noted that the axial displacements measured from the top load platen to the bottom load platen by the DCDTs were different from the extensometer data determined by DIC which was measured from center of the top aluminum ring to center of the bottom aluminum ring. Specifically, the DCDT-measured axial displacements were smaller than the DIC-measured axial displacements. Therefore, it was decided to reload NDL-1 a second time to collect more data to determine the source of this discrepancy. In addition, it was determined that valuable data could be gathered regarding the repeatability of the response of NDL-1; therefore, it was decided to load the test article to failure a second time. Since the second test to failure, or TTF-2, was unplanned, only DCDTs and two low-speed DIC camera systems were utilized. It was later determined that the axial displacement of the barrel was underestimated due to deformation of the loading platen along with the positioning of the DCDTs. For this reason, the end shortening measured from the center of the top aluminum ring and the bottom aluminum ring from the DIC data is presented.

The NDL-1 reached a peak load of 390.4 kips during TTF-2 at an axial displacement of 0.073 in. The radial displacements, axial strains, and hoop strains just prior to failure are shown in Figure 7a, Figure 7b, and Figure 7c, respectively. The damage observed after TTF-1 can be seen in the radial displacement plot and hoop strain plot (Figure 7a and Figure 7c) at 170 degrees, midheight. The feature in the axial strain plot (Figure 7b) at midheight and a circumferential position of 15 degrees is associated with a strain gage wire that came off due to the buckling event in TTF-1 and is therefore not indicative of strain in the test article. As seen in Figure 7a, the maximum inward radial deformation occurs at 30 degrees, 5 in. below the midheight. It is suspected that failure initiated at this dimple. Unlike the buckling location in TTF-1, this dimple does not seem to be associated with any features in the midsurface imperfections or thickness variations in Figure 2 and Figure 3. The maximum hoop strain just prior to failure in TTF-2 occurs approximately at 0 degrees, 10-in. aft of the midheight. While the maximum hoop strain is 7556 $\mu\varepsilon$, which is greater than calculated failure strains based on maximum strain criterion in Table 2, the location the maximum strain is different from the location with the maximum inward radial deformation. The maximum axial strain is well below the calculated failure strain.

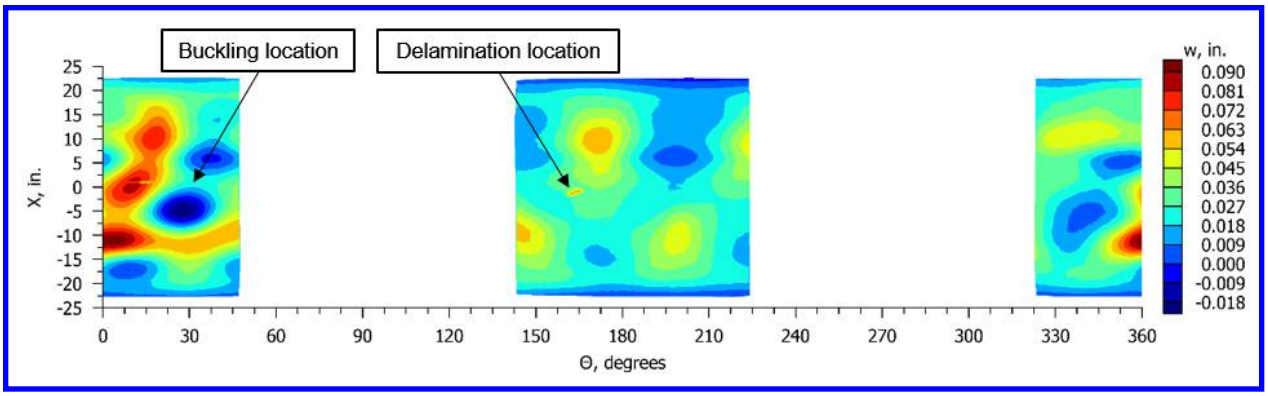

a.) Radial displacements.

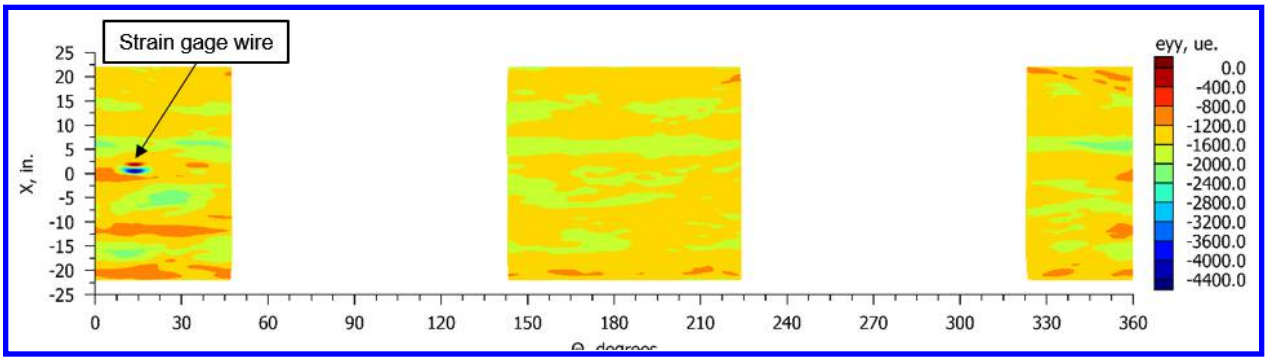

b. Axial strain.

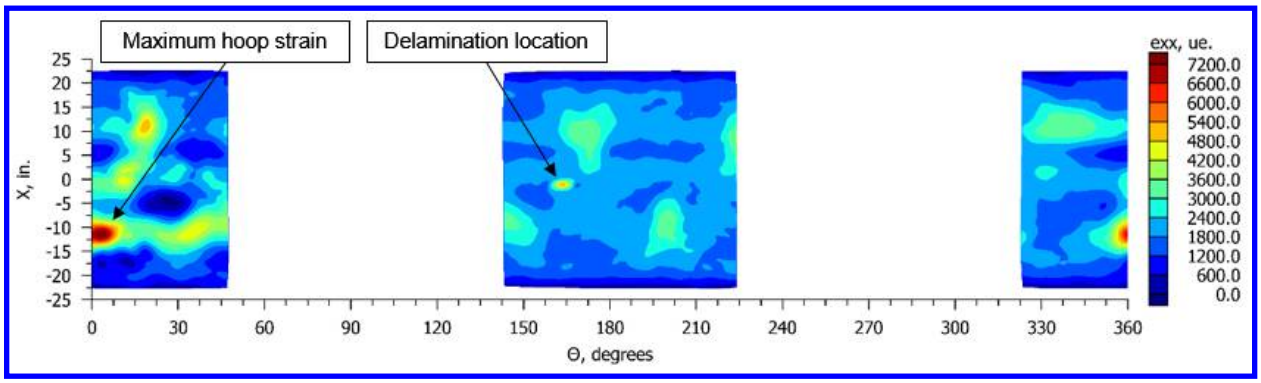

c.) Hoop strain.

Figure 7. NDL-1 at TTF-2 incipient failure.

The damage after TTF-2 was more substantial than the delamination from TTF-1. A V-shaped crack, which penetrated through the thickness of the test article, appears to be in the same orientation as the 23-degree plies, Figure 8. The shape of the crack implies that material failure initiated at the bottom of the "V" and the cracks propagated towards the forward end of the test article. The bottom of the V-shaped crack is centered on the blue dimple, which is located at a circumferential position of 30 degrees and centered at approximately 17.5 in. below the midheight of the test article, as shown in the DIC contour of the radial displacements just after failure (Figure 9). Given the fact that the most inward radial deformation just prior to buckling, the maximum strain just prior to buckling, and the material failure observed posttest did not all occur in the same location, it was concluded that the test article failed in buckling.

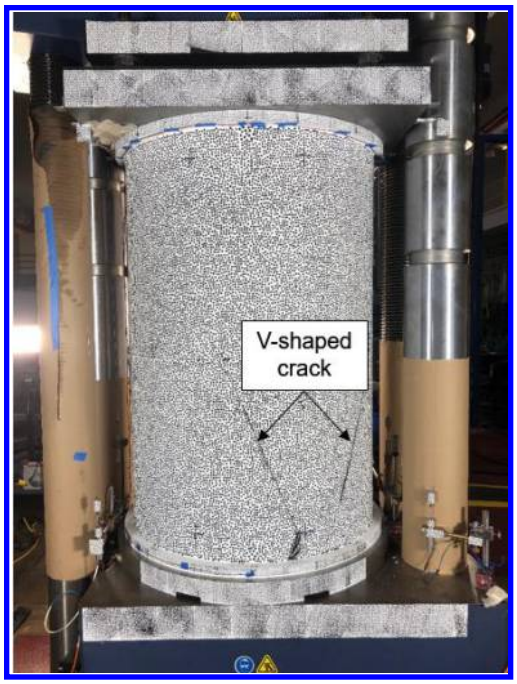

Figure 8. Damage due to the TTF-2 buckling event.

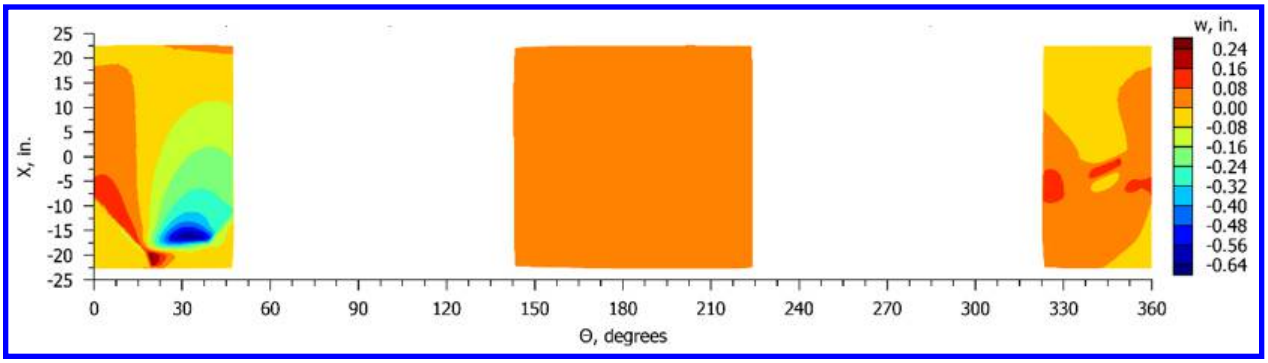

Figure 9. Radial displacements after the buckling event from TTF-2.

C. Comparison of Failure Tests

In general, the test article maintained a majority of its structural integrity despite the first buckling test (TTF-1) and associated material failure. The stiffness was nearly unchanged between TTF-1 and TTF-2. However, there is a slight nonlinearity present in the TTF-2 load versus end shortening curve, Figure 10. During TTF-1, the test article failed in a global buckling event at a load of 466.3 kips at 200 degrees approximately 5 in. above midheight. During TTF-2, the test article carried a maximum axial load of 390.4 kips, approximately 16.3% less than TTF-1, and buckling occurred at approximately the 30-degree circumferential location, 5 in. below the midheight.

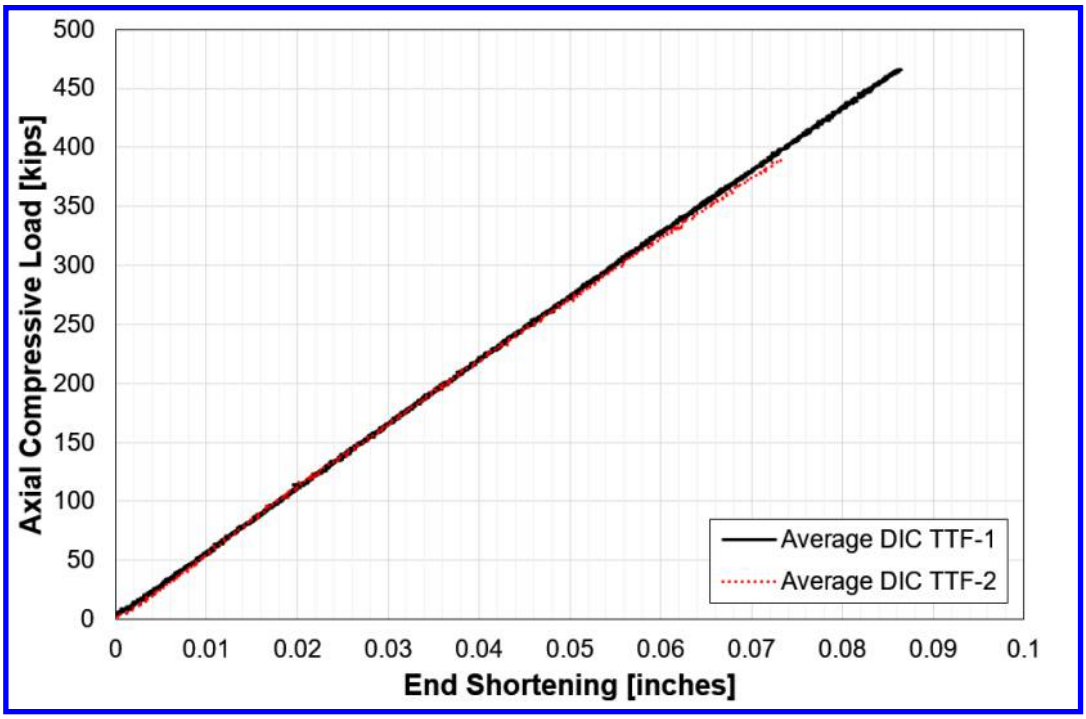

Figure 10. Axial compressive load versus end shortening for TTF-1 and TTF-2.

Comparison of the low-speed DIC data leading up to failure for TTF-1 and TTF-2, shows that the prebuckling shapes are relatively consistent, Figure 5a and Figure 7a. The same dimple pattern appears between 330 degrees and 30 degrees. A major difference is that the dimples that began to form just prior to buckling in TTF-1 begin to take shape at much lower load levels in TTF-2. The radial displacements at 150 kips during TTF-1 and TTF-2 are shown in Figure 11a and Figure 11b, respectively. In Figure 11a, the prebuckling shape has not yet developed at 150 kips during TTF-1. On the other hand, in Figure 11b there are three (3) outward dimples vertically aligned at the 15-degree circumferential position, coinciding with a similar feature observed just prior to buckling in TTF-1, Figure 5a.

In addition, the growth of the radial displacement is greater in TTF-2 than in TTF-1. Referring to Figure 5a, the radial displacements prior to buckling at 466.3 kip during TTF-1, the most inward dimple measured -0.013 in, whereas the most inward dimple measures -0.024 in. just prior to a buckling load of 390.4 kips during TTF-2 (Figure 7a). It is thought that the increased growth of the radial deformations in TTF-2 may have contributed to the nonlinearity present in the load versus displacement curve and for the decrease in load carrying capability.

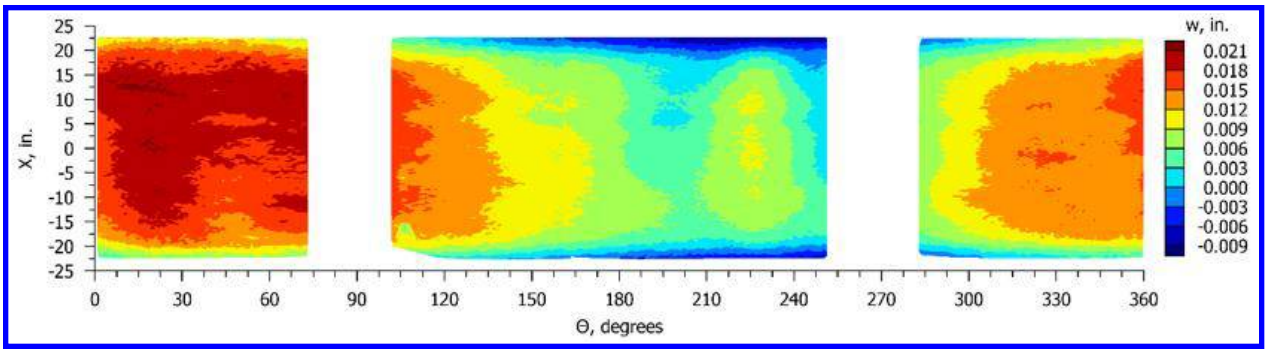

a.) TTF-1.

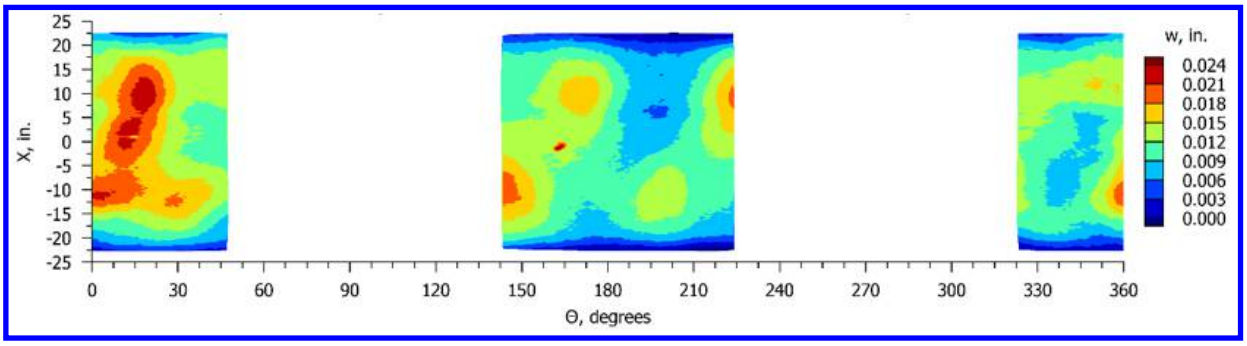

b.) TTF-2

Figure 11. NDL-1 radial deformations at 150 kips.

IV. Conclusion

Composite test article NDL-1 was tested to failure twice. The first series of load sequences was to interrogate the prebuckling, buckling, and postbuckling behavior of the NDL-1 through a series of subcritical load sequences prior to the failure load test. The second test to failure (TTF-2) opportunity arose to investigate a discrepancy between the axial shortening data from the DCDTs and DIC, but it was decided valuable data could be obtained to assess the potential repeatability of the first buckling test. It was concluded that NDL-1 failed in buckling in both TTF-1 and TTF-2. NDL-1 buckled at 466.3 kips during TTF-1, and buckled at a load 16.3% lower in TTF-2 at 390.4 kips. Buckling initiated at different locations in TTF-1 and TTF-2. In TTF-1 buckling occurred at a circumferential position of 200 degrees and 5 in. above the midheight, and a circumferential position of 30 degrees and 5 in. below the midheight during TTF-2. Comparing the radial displacement plots just prior to buckling in TTF-1 and TTF-2, it was observed that the magnitudes were very similar even though NDL-1 buckled a lower load in TTF-2. Therefore, the rate of growth of the radial displacement was larger in TTF-2. It is postulated that this radial-displacement behavior potentially contributed to nonlinearity seen in the load versus displacement plot and the reduction in load carrying capability during TTF-2. NDL-1 was able to carry 83.7% of its original load capacity and the prebuckling deformation shapes were similar during the second test to failure. Even though NDL-1 was not originally designed or analyzed for two buckling failure tests, it did demonstrate a level of repeatability between the first and second failure tests.

Acknowledgments

The authors would like to thank Ines Uriol Balbin, for the test-article design work, Kevin van Dooren for analysis support, and David Eberlein for the pretest predictions and posttest analysis correlation, all associated with the Delft University of Technology. In addition, Dr. Cyrus Kosztowny from NASA Langley Research Center for creating the midsurface and radial imperfection plots. The work described in this report was conducted as part of the NASA Engineering and Safety Center (NESC) Shell Buckling Knockdown Factor Project, NESC assessment number 07-010-E, in collaboration with the Delft University of Technology.

References

[1] Uriol Balbin, I., Bisagni, C., Schultz, M.R., and Hilburger, M.W., "Scaling Methodology Applied to Buckling of Sandwich Composite Cylindrical Shells." *AIAA Journal*, Vol. 58, No. 8, 2020, pp. 1-10.

[2] Hexcel Corporation, "HexPly® 8552 Epoxy Matrix (180°C/365°F) curing matrix product data sheet." https://www.hexcel.com/user_area/content_media/raw/HexPly_8552_eu_DataSheet.pdf, accessed May 27, 2020.

[3] Clarkson, E., Hexcel 8552 IM7 unidirectional prepreg 190 gsm & 35%RC qualification statistical analysis report. Technical Report NCP-RP-2009-028 Rev N/C, National Institute for Aviation Research, Wichita, Kansas, USA, 2011.

[4] Eberlein, D. J., "Composite Cylindrical Shell Buckling: Simulation & Experimental Correlation," Master's Thesis, Faculty of Aerospace Engineering, Delft University of Technology, Delft, Netherlands, 2019.